RESEARCH ARTICLE

EARTH SCIENCES

Dissecting the contributions of organic nitrogen aerosols to global atmospheric nitrogen deposition and implications for ecosystems

Authors

Yumin Li[1,2,3], Tzung-May Fu[1,2,4]*, Jian Zhen Yu[3,5]*, Xu Yu[3], Qi Chen[6], Ruqian Miao[6], Yang Zhou[7,8], Aoxing Zhang[1,2], Jianhuai Ye[1,2], Xin Yang[1,2], Shu Tao[1,2], Hongbin Liu[9], Weiqi Yao[10]

Affiliations

[1]Shenzhen Key Laboratory of Precision Measurement and Early Warning Technology for Urban Environmental Health Risks, School of Environmental Science and Engineering, Southern University of Science and Technology, Shenzhen, 518055, China.

[2]Guangdong Provincial Observation and Research Station for Coastal Atmosphere and Climate of the Greater Bay Area, Southern University of Science and Technology, Shenzhen, 518055, China.

[3]Division of Environment and Sustainability, Hong Kong University of Science and Technology, Hong Kong, 999077, China.

[4]National Center for Applied Mathematics Shenzhen, Shenzhen, 518055, China.

[5]Department of Chemistry, Hong Kong University of Science and Technology, Hong Kong, 999077, China.

[6]State Key Joint Laboratory of Environmental Simulation and Pollution Control, International Joint laboratory for Regional Pollution Control, College of Environmental Sciences and Engineering, Peking University, Beijing, 100871, China.

[7]Frontier Science Center for Deep Ocean Multispheres and Earth System and Physical Oceanography Laboratory, Ocean University of China, Qingdao, 266100, China

[8]College of Oceanic and Atmospheric Sciences, Ocean University of China, Qingdao, 266100, China

[9]Department of Ocean Science, Hong Kong University of Science and Technology, Hong Kong, 999077, China.

[10]Department of Ocean Science and Engineering, Southern University of Science and Technology, Shenzhen, 518055, China.

* Corresponding authors: Tzung-May Fu, Jian Zhen Yu

Email: fuzm@sustech.edu.cn; chjianyu@ust.hk

Abstract

Atmospheric deposition of particulate organic nitrogen (ON_p) is a significant process in the global nitrogen cycle and may be pivotally important for N-limited ecosystems. However, past models largely overlooked the spatial and chemical inhomogeneity of atmospheric ON_p and were thus deficient in assessing global ON_p impacts. We constructed a comprehensive global model of atmospheric gaseous and particulate organic nitrogen (ON), including latest knowledge on emissions and secondary formations. Using this model, we simulated global atmospheric ON_p abundances consistent with observations. Our estimated global atmospheric ON deposition was 26 Tg N yr^{-1}, predominantly in the form of ON_p (23 Tg N yr^{-1}) and mostly from wildfires (37%), oceans (22%), and aqueous productions (17%). Globally, ON_p contributed as high as 40% to 80% of the total N deposition downwind of biomass burning regions. Atmospheric ON_p deposition thus constituted the dominant external N supply to the N-limited boreal forests, tundras, and the Arctic Ocean, and its importance may amplify in a future warming climate.

Keywords

Organic nitrogen aerosol, Secondary organic nitrogen, Biomass burning.

MAIN TEXT

Introduction

Organic nitrogen (ON) refers to the nitrogen (N) atoms covalently bound to organic molecules. ON in the atmosphere includes a wide variety of reduced and oxidized species [1, 2] and has profound impacts on the biogeochemical cycle of nitrogen and on climate [3-8]. Atmospheric deposition of total N (TN), including both inorganic nitrogen (IN) and ON components, is estimated to be 77 to 135 Tg N yr^{-1} [9-11] and constitutes an important external source of nutrient to terrestrial and marine ecosystems. Observations have shown that, on average, 25% of the atmospheric TN deposition is organic, primarily in the form of particulate ON (ON_p) (Supplementary Material: Datasets S1 and S3). However, there are large regional and seasonal variations in the organic fractions of atmospheric TN deposition, yet the reasons for these variations are not well understood [2, 12]. Moreover, the bioavailability of ON_p species to different terrestrial and marine primary producers ranges widely between 2% and 80% [6, 13-17], while chronic exposure to some atmospheric ON_p species (e.g., quinoline) are toxic to terrestrial plants and marine plankton [1]. Atmospheric ON_p is also thought to be the dominant colored component of atmospheric brown carbon aerosol [18, 19], affecting the radiative balance of Earth's climate system [8, 20]. However, the global environmental impacts of atmospheric ON_p remain underdiagnosed, because their global sources, abundances, compositions, and depositions are not well quantified.

Atmospheric ON_p may be directly emitted from anthropogenic [21] and biomass burning [22] activities and as constituent substances present in sea spray aerosol [23], dust [24], and primary biological atmospheric particulates [23], collectively referred to as primary ON_p (PON_p). In addition, secondary ON_p (SON_p) may be produced in the atmosphere

from multiple pathways, including most importantly (Fig. 1): (1) via the gas-phase oxidation of aliphatic volatile organic compounds (VOCs) by OH or NO_3 radicals in the presence of nitrogen oxides ($NO_x \equiv NO + NO_2$) to form semi-volatile organic nitrates, which are then irreversibly up-taken at the surface of wet aerosols [25, 26]; (2) via the gas-phase oxidation of aromatic VOCs by OH or NO_3 radicals in the presence of NO_x to form semi-volatile nitroaromatics, which partition into the particulate phase [27-29]; and (3) via the aqueous reactions of dicarbonyls with ammonium or amines in cloud droplets and wet aerosols to from heterocyclic compounds with imine or amine functional groups (e.g., imidazoles, imidazole-2-carboxaldehyde, and pyrroles) [30-34]. Previous modeling studies estimated global PON_p abundances by scaling primary organic carbon aerosol with observed N:C molar ratios, but those studies did not distinguish the N:C ratios from different biomass burning and anthropogenic sources [10, 11, 35, 36]. Previous studies also estimated SON_p by scaling secondary organic aerosol (SOA) with N:C ratios, by scaling ammonium abundance, or by simulating simple formation of organic nitrates from the oxidation of biogenic VOCs at prescribed yields [10, 11, 35, 36]. Their simulated atmospheric ON_p deposition fluxes under-predicted the observations by an order of magnitude at sites with high ON deposition fluxes, unless *ad hoc* scaling was applied [10, 11, 35, 36]. Furthermore, previous studies have not evaluated their simulated atmospheric ON_p concentrations against measurements.

We presented here a comprehensive global simulation of atmospheric ON for the year 2016, built on the GEOS-Chem 3-D chemical transport model (v12.9.3, http://geos-chem.org) at 5° longitude $\times$ 4° latitude resolution [37]. We incorporated the current-best knowledge of the primary sources of gaseous ON (ON_g) and ON_p species and their N:C mass ratios, the explicit formation pathways of SON_p (Fig. 1), as well as the chemical aging processes of ON_g and ON_p in the atmosphere (Materials and Methods;

Supplementary Material: Text S1). We evaluated our simulated atmospheric ON_p abundances and deposition fluxes against global measurements and analyzed the simulated spatiotemporal and source variabilities of atmospheric ON_p deposition, with the goal of better quantifying the resulting external N supply to the global ecosystems.

Results and Discussion

Simulated global atmospheric ON_p abundance, spatiotemporal variability, and source attribution

Figures 2, S1, and S2 compare our simulated global annual mean surface concentrations of ON_p and fine ON_p (particulate ON with aerodynamic diameters <2.5 μm, ON_{fp}) against observations at global surface sites between the years 1999 and 2020 (Supplementary Material: Dataset S1). We combined measurements of ON_p and the water-soluble part of ON_p ($WSON_p$) reported in the literature, because measurements showed most ON_p to be soluble, except for the ON_p sampled at some marine and dust-affected sites. We also focused below on the evaluation of simulated ON_{fp}, because most measurements only sampled fine particles; in the few studies where both fine and coarse particles were measured, the observed ON_p was predominantly in the fine particles. Observed ON_{fp} concentrations at global sites ranged between 0.01 and 30 μg N m^{-3} (global average 0.47 μg N m^{-3}, excluding three extremely high ON_{fp} observations affected by local sources), with higher concentrations at sites affected by biomass burning and anthropogenic sources and generally lower concentrations at remote marine sites. Our simulated ON_{fp} concentrations matched the observed magnitudes and spatial distributions of surface ON_{fp} with no apparent systematic biases (Fig. 2B, slope = 1.0 ± 0.4, correlation coefficient R = 0.6). We also evaluated our simulated ON_{fp} against seasonal measurements in Southern China and found that the model reproduced the observed ON_{fp} concentrations and the

enhancements during the cold season (Fig. S3, Dataset S1). Thus, our simulation represented the first successful model depiction of observed global surface ON_{fp} abundance. The model underestimated three extremely high ON_{fp} observations, which sampled during local incineration events of agricultural residues and wastes (Kanpur, India) [38] or during local dust storms (Xi'an and Zhangjiakou, China) [24, 39]. These local, intermittent emitting events were either under-represented in the satellite-based burning activity data or missed by our global simulation for a different year.

The observed concentrations of surface ON_p concentrations were similar to those of ON_{fp} (Fig. S2), because ON_p were mostly in the fine mode. Our simulated global annual mean surface ON_p concentration was 0.23 μg N m^{-3}, also mostly in the form of ON_{fp} (0.19 μg N m^{-3}, 83% of simulated ON_p). Surface ON_{fp} were mostly from biomass burning emissions (0.12 μg N m^{-3}, 63%), secondary production (0.04 μg N m^{-3}, 21%), and anthropogenic emissions (0.02 μg N m^{-3}, 11%) (Figs. S1, S4, and S5). The highest simulated annual mean ON_{fp} concentrations were over the Siberian and tropical forests (1 to 11 μg N m^{-3}), reflecting the emissions of ON_{fp} and its precursors from wildfires. Simulated ON_{fp} concentrations exceeded 0.5 μg N m^{-3} over East Asia, South Asia, and Southeast Asia, due to the pronounced anthropogenic emissions in these regions. Dust (0.003 μg N m^{-3}) and marine (0.009 μg N m^{-3}) contributions to ON_{fp} were relatively small because these sources emitted ON_p mainly as coarse particles.

SON_p contributed >20% of the simulated ON_{fp} concentrations at approximately one-third of the surface sites, especially at locations with high ON_{fp} concentrations (Figs. 2B, S1, and S4). The simulated global SON_p predominantly consisted of imine SON_p, produced via the aqueous reaction of dicarbonyls with ammonium (Figs. S1 and S4). The simulated annual mean surface imine SON_p concentrations exceeded 0.1 μg N m^{-3} in East and South

Asia, Southeast U.S., the boreal forests, and the rainforests of Africa and South America, reflecting the emissions of dicarbonyls and their precursors from anthropogenic, biomass burning, and biogenic activities [40, 41]. In our model, organic nitrate SON_p and nitroaromatics SON_p each contributed less than 0.001 μg N m^{-3} (0.5%) of the global mean surface ON_{fp}, respectively. The spatial distributions of SON_p from all three secondary formation pathways were similar due to their common precursor sources (Fig. S4).

We further evaluated our simulated SON_p compositions against the limited measurements of particulate nitroaromatics and organic nitrates currently available (Supplementary Material: Dataset S2). Our simulated nitroaromatic SON_p concentrations (0.005 to 78 ng N m^{-3}) were consistent with the observed abundance and spatial distribution of particulate nitroaromatics (0.09 to 250 ng N m^{-3}, R = 0.6, Figs. S4I and S6). Observations showed that molecules containing organic nitrate functional groups comprised 4% to 28% and 2% to 25% of the ambient surface organic aerosol mass in China [42-44] and in the U.S. [45, 46], respectively (Dataset S2). Assuming a typical molecular weight of 250 g mole^{-1} (corresponding to organic nitrate molecules with N:C mass ratios of 0.1 to 0.5) [46], our simulated particulate organic nitrates comprised 3% to 27% and 5% to 24% of the simulated surface organic aerosol mass in China and in the U.S., respectively, consistent with the observations. Our simulated organic nitrate SON_p concentrations (0.005 to 300 ng N m^{-3}) were consistent within an order of magnitude against most particulate organic nitrate observations over North America and Asian sites, but the simulated concentrations were systematically lower than the observations in Europe (Figs. S4H and S7). However, those mass spectrometry-based particulate organic nitrate measurements in Europe might have been biased high, because the researchers attributed a larger fraction of the total detected nitrate fragments to organic nitrates by assuming a large NO_2^+ to NO^+ fragment ratio for organic nitrates (0.1) [47, 48]. On the other hand, it was also possible that our

simulated particulate organic nitrate concentrations were biased low. Observations showed that particulate organic nitrates in Europe were mostly formed from the nighttime biogenic VOC oxidation by NO_3 [47]. Chamber experiments and ambient measurements showed that the molar yields of particulate organic nitrates from isoprene-NO_3 oxidation were between 4% and 24% [49], while the molar yields of particulate organic nitrates from monoterpene-NO_3 oxidation were between 15% and 57% [50, 51]. In our simulation, the molar yields of gaseous organic nitrates from VOC-NO_3 reactions and the uptake coefficient of gaseous organic nitrates by aqueous particles were fitted to the ambient observations in the Southeast U.S. [26], resulting in overall global particulate organic nitrate yields of 22% from isoprene-NO_3 reactions and 9% from monoterpenes-NO_3 reactions. Thus, our simulated production of particulate organic nitrates from monoterpenes may be low and lead to organic nitrate underestimation over Europe, since that pathway was a larger contributor to organic nitrates in Europe than it was in China and U.S. Furthermore, we assumed that all particulate organic nitrates in the aqueous phase underwent hydrolysis to form nitric acid at a timescale of an hour, based on a fitting to ambient measurements in the Southeast U.S. [26]. However, chamber experiments found that the lifetimes of organic nitrates against hydrolysis may vary between minutes to weeks, depending on the molecular structure of the organic nitrate species and the pH value of the solution [52-55]. In particular, some organic nitrates from monoterpenes with a ring skeleton containing three delocalized π orbitals hydrolyze slowly at lifetimes exceeding a week [54, 55] , while some non-tertiary nitrates from isoprene do not undergo hydrolysis at all [52, 53]. In addition, recent chamber studies have demonstrated that gas-phase organic nitrates produced from monoterpene oxidation may photolyze at rates 2 to 10 times slower than the photolysis rates we assumed for organic nitrates from

monoterpene (lifetimes against photolysis 1 to 2 hours) [56, 57]; this potential bias may also contribute to our underestimation of particulate organic nitrates.

We evaluated the robustness of our global ON_p abundance estimates by conducting sensitivity experiments, in which the N:C ratios for PON_p emissions and SON_p formation rates were varied within their respective literature-reported ranges (Supplementary Material: Text S2). From these sensitivity experiments, the range of global annual mean surface ON_{fp} concentrations was between 0.06 and 0.32 μg N m^{-3} (ON_p concentrations between 0.08 and 0.36 μg N m^{-3}, Figs. S8 and S9). Coarse ON_p (ON particles >2.5 μm in diameter, ON_{cp}) accounted for less than 25% of total ON_p concentration everywhere except at marine sites, and our varying the N:C emission ratios of primary ON_{cp} had very little impact on the simulated global surface ON_p concentrations. This was consistent with previous observations of atmospheric ON_p being predominantly in the fine mode (Supplementary Material: Dataset S1).

On a global scale, the most variable sources for our simulated ON_p were biomass burning emissions and imine SON_p production. We found that a PON_p-enhanced scenario (with high-end biomass burning N:C emission ratio and low-end imine SON_p formation rates) and an SON_p-enhanced scenario (with low-end biomass burning N:C emission ratio and high-end imine SON_p formation rates) would both produce results similar to our standard simulation and consistent with observed surface ON_p concentrations (Figs. S10 and S11). The simulated mean global surface ON_{fp} concentrations were 0.22 μg N m^{-3} for the PON_p-enhanced scenario and 0.15 μg N m^{-3} for the SON_p-enhanced scenario, respectively, with biomass burning contributing 64% and 7% of the mean global surface ON_{fp} abundance, and imine SON contribute 9% and 74% of the mean global surface ON_{fp} abundance, respectively. However, published observations were deficient in distinguishing these two

scenarios, because there were relatively few measurements in areas strongly affected by biomass burning and no explicit measurements of imine SON_p (Figs. 2 and S1). As a result, our standard simulation may underestimate the contributions of biomass burning PON_p or SON_p to global ON_p abundance, potentially up to a factor of 9.

Evaluation of simulated atmospheric ON deposition flux

Figure 3 evaluates the simulated atmospheric deposition fluxes of ON (including ON_g and ON_p) and the ON:TN ratios in those deposited fluxes against global surface observations (Supplementary Material: Dataset S3). Observations of ON deposition fluxes were subject to significant uncertainty. One-third of the published ON deposition measurements only analyzed dissolved ON (DON) contents and only in rainwater samples, thus they might underrepresent the atmospheric deposition of ON. On the other hand, ON contents were almost always inferred by the measured differences between TN and IN. This technique tended to overestimate ON deposition and its ON:TN ratios, particularly where ON deposition fluxes were low because negative ON measurement was either rounded up to zero or excluded [58, 59]. We compared our model results to all published measurements but noted these technical issues as potential causes for discrepancies between the model and the observations.

Our simulated global atmospheric ON deposition flux was 26 Tg N yr^{-1} (including 2.5 Tg N yr^{-1} of ON_g and 23 Tg N yr^{-1} of ON_p), and the spatial distribution of simulated fluxes was consistent with the observed gradients of ON deposition fluxes from marine (0.01 to 0.99 g N m^{-2} yr^{-1}) to inland (0.07 to 3.8 g N m^{-2} yr^{-1}) sites (Fig. 3). Over land, the model reproduced the observed high ON deposition fluxes over South and East Asia, Western

Europe, the tropical forests of Africa and South America, and the boreal forests of North America and Siberia, reflecting the deposition of atmospheric ON from biomass burning and anthropogenic sources (Figs. 3 and 4). Over the ocean, the observed and simulated ON deposition fluxes both showed enhancements downwind of areas with pronounced biomass burning, anthropogenic, and dust emissions, as well as over locations with enhanced marine ON emissions. Overall, our simulated ON deposition fluxes were lower than the observed ON deposition fluxes by a factor of 3 (Fig. 3B), an improvement over previous model studies that underestimated the observed ON deposition fluxes by more than one order of magnitude, especially at sites with high ON deposition fluxes [10, 11, 35, 36]. This improved representation of atmospheric ON deposition relative to previous studies was driven by a combination of model improvements: our use of updated, source-specific N:C ratios for primary ON_{fp} from biomass burning and anthropogenic combustion, the use of updated N:C ratios for ON_{cp} from marine and dust emissions, as well as the explicit inclusion of imine SON_p formations. Varying the N:C emission ratios for ON_{cp} within the literature-reported ranges led to simulated global ON_{cp} deposition fluxes between 4.5 and 8.9 Tg N yr^{-1} (Supplementary Material: Text S2); our selected high-end N:C emission ratios for ON_{cp} conformed with the observed deposition fluxes. Our simulation showed that SON_p contributed >20% of the atmospheric ON deposition fluxes in one-third of the observed sites, particularly at forested, urban, and rural locations.

Figures 3C and 3D compare the simulated and observed ON:TN ratios in the atmospheric deposition fluxes. The observed ON:TN ratios averaged 25% globally but showed wide-ranging regional variability between 2% and 70% (Supplementary Material: Dataset S3). Our simulated ON:TN deposition ratios at the observation sites ranged between 3% and 50% with a global average of 21%. Observed ON:TN ratios in deposition fluxes at a

single site varied by a factor of 2 to 5, partially reflecting the measurement uncertainties described above and partially reflecting the interannual variation of observations. On a site-by-site basis, the discrepancies between our simulated ON:TN ratios and the observations were mostly within a factor of 5 (Fig. 3D). Therefore, our simulated ON:TN ratios agreed with the observations within the uncertainties of observations. These comparisons represented the first site-by-site evaluation of global simulated ON:TN deposition ratios and indicated that our model was capable of simulating the atmospheric N deposition fluxes and the ON contributions to global ecosystems.

To test the robustness of our simulations, we analyzed the results from the sensitivity experiments where N:C ratios for PON_p and production rates of SON_p were varied within their literature-reported ranges (Supplementary Material: Text S2; Figs. S13 to S16). In these sensitivity experiments, the simulated global ON deposition flux ranged between 10 and 40 Tg N yr^{-1}, with ON contributing 9% to 29% of the global TN deposition. SON_p contributed 6% to 61% of the total ON deposition. We found that the experiment with an upper-limit N:C ratio for PON_p and the fastest production for SON_p would still underestimate the observed ON deposition fluxes by a factor of two (Fig. S13), especially in the high-ON_p regions. These discrepancies indicated potential underestimation of the biomass burning and anthropogenic emissions of PON_p or SON_p precursors.

We conducted further sensitivity tests to fit the simulated ON deposition fluxes against the observations by increasing the PON_p emissions from anthropogenic and biomass burning sources, and by increasing the imine SON_p production (Fig. S18). We found that increasing the anthropogenic PON_p emissions by a factor of 9 would result in good agreement between the simulated and observed ON deposition fluxes but would lead to an overestimation of surface ON_{fp} abundance by a factor of 4. In contrast, increasing biomass

burning PON_p emissions or imine SON_p production by a factor of 5, respectively, would both result in good agreements between the simulated and observed ON deposition fluxes, while the simulated surface ON_{fp} concentrations would only be larger than current observations by a factor of 2. These findings again confirmed that ON_p from biomass burning, and secondary productions may be biased low in our standard simulation, and that further measurements representing these sources are need to better constrain the global abundance and deposition fluxes of ON.

Global budget of atmospheric ON and contribution to atmospheric TN deposition

Table 1 summarizes the global budget of atmospheric ON as simulated by our model. The total atmospheric burden of ON was 1.3 Tg N (range in sensitivity experiments was 1.1 Tg N to 1.5 Tg N), including 1.0 Tg N of ON_g and 0.3 Tg N of ON_p. ON_g species were mostly chemically produced in the atmosphere as acyl peroxy nitrates (e.g., peroxyacetyl nitrate) and non-acyl peroxy nitrates (e.g., methyl peroxy nitrate), and all ON_g species had limited solubility [2]. As such, ON_g were mainly removed from the atmosphere by thermal decomposition, photolysis, or OH oxidation [26, 60], with deposition accounting for a mere 1% to 2% of its global sink [61]. Globally, ON_g only constituted 9% of the total atmospheric ON deposition. In contrast, ON_p constituted only 23% of the global atmospheric ON burden but dominated the global atmospheric ON deposition (91%). Of the 0.3 Tg N global atmospheric ON_p burden, 87% (0.26 Tg N) was in the fine mode (ON_{fp}). ON_{cp} constituted only 13% (0.04 Tg N) of the global ON_p burden because of its rapid deposition. Globally, biomass burning (8.5 Tg N yr^{-1}) and anthropogenic (1.3 Tg N yr^{-1}) emissions were the most important primary sources of ON_{fp}, while marine emissions were the dominant primary source of ON_{cp}. Net secondary production constituted an

atmospheric ON_p source of 3.9 Tg N yr^{-1}, 97% of which was associated with the aqueous reaction of dicarbonyls with ammonium to form imine SON_p.

Figure 5 illustrates the contributions of different N components to the global atmospheric TN deposition. Our simulated global atmospheric TN deposition flux was 124 Tg N yr^{-1}, including 78 Tg N yr^{-1} and 46 Tg N yr^{-1} to the global terrestrial and marine ecosystems, respectively. On a global scale, IN and ON each contributed 79% (98 Tg N yr^{-1}) and 21% (26 Tg N yr^{-1}) of the atmospheric TN deposition, respectively. Deposition of atmospheric ON was mostly through wet scavenging (20 Tg N yr^{-1}) and less through dry deposition (6.0 Tg N yr^{-1}), because the dominant depositing component, ON_p, was highly water-soluble. In contrast, the dry and wet deposition fluxes of IN were comparable in magnitudes, because the dry deposition of gaseous IN species was more efficient than that of gaseous ON species. Overall, the atmospheric deposition fluxes of ON_p (23 Tg N yr^{-1}) constituted of 19 Tg N yr^{-1} PON_p (including 8.5 Tg N yr^{-1} from biomass burning, 5.0 Tg N yr^{-1} from marine emissions, and 1.3 Tg N yr^{-1} from anthropogenic emissions) and 3.9 Tg N yr^{-1} SON_p, each contributing 83% and 17% of the global atmospheric ON_p deposition, respectively. Primary and secondary ON_p each constituted 16% and 3% of the global atmospheric TN deposition, respectively.

Previous model estimates for the atmospheric ON deposition fluxes, without applying *ad hoc* scaling, was between 10 and 32 Tg N yr^{-1}, but their simulated atmospheric ON deposition fluxes were lower than observations by one order of magnitude, especially at high-ON locations [10, 11, 35, 36]. In comparison to our simulated global ON budget, we found that the discrepancy between previous model studies and observations arose from two aspects. Firstly, previous model studies emitted larger amounts of ON_p from marine sources and PBAPs, such that more than half of their global atmospheric ON_p deposition

was due to the deposition of these natural ON_p species, but their simulated deposition fluxes were still lower than the observations at the high-ON locations affected by anthropogenic and biomass burning activities. Secondly, previous studies estimated a larger deposition flux of ON_g, because they assumed all ON_g species were soluble. As such, previous studies attributed 30% of global atmospheric ON deposition to ON_g [10]. In terms of the origins of ON_{fp}, previous assessments estimated the combined deposition flux of anthropogenic and biomass burning PON_p to be 8 to 15 Tg N yr^{-1}, with PON_p being largely from anthropogenic sources [10, 11, 35, 36]. We showed that the global abundance and deposition of PON_p were predominantly from biomass burning, for which our estimated emissions may still be too low. Increasing the anthropogenic source of PON_p in our model to match the observed deposition fluxes would led to severe overestimation of the observed surface ON_p concentrations (Fig. S18). In addition, previous studies estimated the atmospheric deposition flux of SON_p to be 2 to 18 Tg N yr^{-1}, 30% to 100% of which consisted of oxidized SON_p [10, 11, 35, 36]. Our simulation indicated that the global atmospheric SON_p was predominantly imine-like, reduced ON species produced from the aqueous-phase reactions of dicarbonyls and ammonium.

Impacts of spatially inhomogeneous atmospheric ON_p deposition on global ecosystems

Our simulation showed that the ON:TN ratios in atmospheric deposition fluxes have strong geographical variabilities that were closely related to the regional sources of ON, which would also affect the chemical composition of deposited ON. Global terrestrial and marine ecosystems are distinctly limited by N or other nutrients [4, 62]. In addition, laboratory studies showed that the bioavailability of different ON species, i.e., the percentage of ON mass that can be assimilated by primary producers, ranged between 2%

and 80% for bulk PON_p from different sources with large uncertainty [6, 13-17], while the reduced ON_p species (e.g., imines) were almost entirely bioavailable (Supplementary Material: Text S3) [63]. Therefore, the ecological impacts of atmospheric ON deposition may be regionally disparate.

Our simulated spatial and chemical inhomogeneity of atmospheric ON deposition indeed led to great variability in the effective bioavailability of ON deposited to global ecosystems (Fig. 6; Supplementary Material: Text S3). Our calculations showed that atmospheric ON deposited over East Asia, Southeast Asia, Europe, the Pacific, and North Atlantic were of higher bioavailability, because the ON deposited over these areas contained large fractions of imine SON_p. In contrast, the atmospheric ON deposited over the arid areas of Africa, Middle East, Australia, and South America were predominantly from dust and of lower bioavailability (Fig. 4).

We highlight two types of regions: (1) regions near and downwind of biomass burning emissions, and (2) regions near and downwind of anthropogenic sources. Over ecosystems near and downwind of biomass burning emissions, including the boreal forests and tundra, the tropical forests, the tropical Atlantic, and the Arctic Ocean, the simulated atmospheric ON deposition fluxes exceeded 0.1 g N m^{-2} yr^{-1}. The simulated deposited ON:TN ratios ranged from 40% to 80%, which were the highest values globally and consistent with the limited observations of atmospheric deposited ON:TN ratios at biomass burning-affected forest sites (observed values between 19% and 70% with an average of 41%; Supplementary Material: Dataset S3). We calculated that the effective bioavailability of ON deposited over these areas was 50% (sensitivity calculations ranged 34% to 87%), such that ON may potentially contribute 14% to 70% of the atmosphere-supplied bioavailable N into these ecosystems (Fig. 6; Supplementary Material: Text S3).

The ecological impacts of atmospheric ON deposition may be pivotal over these areas, if N was the local limiting nutrient and other external N inputs were small. This finding was consistent with previous studies which showed that the biogeochemical cycling of N in primeval forests was mainly driven by the ON emissions and depositions associated with biomass burning [3, 64], especially in boreal regions [6]. Our simulations further showed that, in these boreal forests, tundra, and tropical forests affected by biomass burning, 20% to 60% of the deposited ON_p were secondary and chemically reduced (Fig. 4). This finding suggests that atmospheric deposition of reduced ON_p may play an important role in the biogeochemistry of these ecosystems, especially in the N-limited boreal forest and tundra [62], but that biogeochemical role of atmospheric ON has not been fully explored. Similarly, marine ecosystems in the Arctic Ocean and the tropical Atlantic are receptors of biomass burning ON_p long-range transported from the boreal forest and Africa, respectively. The impacts of atmospheric ON deposition on productivity in these ecosystems are complex, as the biological assimilation of N in oceans is tightly coupled to other essential nutrients (such as iron and phosphorus) and temperature [4, 65]. In the Arctic Ocean, where primary production is known to be N-limited in summer [66, 67], atmospheric deposition of ON constituted a large external N source and may increase regional primary productivity. Microbial species capable of assimilating the deposited atmospheric ON potentially have a competitive advantage there [63, 68].

Over regions strongly affected by anthropogenic sources, including East and South Asia, Europe, Northwestern North Pacific, and the North Indian Ocean, the simulated ON:TN ratios were typically below 20% due to the abundant anthropogenic IN in the regional atmosphere (Fig. 4). However, the simulated atmospheric ON deposition fluxes over these regions were still large (>0.1 g N m^{-2} yr^{-1}), and 20% to 40% of the deposited ON fluxes were secondary and chemically reduced. Furthermore, the ON deposited over these

regions were highly bioavailable (50% to 90% effective bioavailability, Fig. 6; Supplementary Material: Text S3). The marine ecosystems of Northwestern Pacific and the North Indian Ocean are also known to be N-limited [4], such that the deposition of atmospheric ON, particularly the more bioavailable, reduced ON, may have large impacts there.

Discussions

Our simulated atmospheric ON_p abundance and ON deposition fluxes were consistent with most available observations, although there remained a factor of 3 discrepancy between our simulated global atmospheric ON deposition fluxes and observations. We showed that increases in the biomass burning emissions of PON_p or the production of SON_p may help close that discrepancy, highlighting the need for targeted ambient measurements in biomass burning-affected areas and the abundance and chemical composition of SON_p to better constrain these sources.

In a future warming climate, wildfires will likely intensify and become more frequent [69], increasing their emissions of both PON_p and precursors of SON_p. Meanwhile, anthropogenic emissions of nitrogen oxides will continue to decrease in the future, reducing the abundance of oxidized IN in the atmosphere and its deposition [70]. A warming climate will also lead to more pronounced thermal stratification of the surface ocean, enhancing the importance of atmospheric N deposition as an external N source to the surface marine ecosystems [71]. Atmospheric ON deposition may become an increasingly important external N source to global terrestrial and marine ecosystems, and its impacts warrant further investigations.

Materials and Methods

Detailed descriptions of all methods and materials are presented in the Supplementary Material. Briefly, we developed a global atmospheric gaseous and particulate ON simulation for the year 2016 using the GEOS-Chem global 3-D chemical transport model (v12.9.3, http://geos-chem.org) [37] at a horizontal resolution of 5° longitude $\times$ 4° latitude and with 72 vertical layers. The simulation represented the primary emissions of atmospheric particulate and gaseous ON, the formation pathways of gaseous and particulate secondary ON in the atmosphere, and chemical aging of gaseous and particulate ON (Supplementary Material: Text S1). We conducted sensitivity simulations to evaluate the impacts of emission ratios and chemical parameters on the global budget of ON_p (Supplementary Material: Text S2). We calculated the bioavailability of atmospherically deposited ON fluxes to primary producers (Supplementary Material: Text S3). Published observations of atmospheric ON_p concentrations and atmospheric ON deposition fluxes are described and compiled in Datasets S1, S2, and S3. Each dataset includes a complete list of references to the observational studies.

Data and materials availability: All data are available in the main text or the supplementary materials. The GEOS-Chem model code used in this study is permanently archived at https://www.scidb.cn/en/s/iuUvUj (Link currently for review only and will become publicly available upon publication).

Author contributions:

T.M.F designed conception of the research. Y.L, T.M.F., J.Z.Y, X.Yu, Q.C, R.M, A.Z, H.L and W.Y developed the methodology. Y.L, T.M.F, J.Z.Y, Y.Z, A.Z, J.Y, X.Yang and S.T made the investigation. Y.L, T.M.F made the visualization. Y.L and T.M.F wrote the manuscript with input from all co-authors. T.M.F, J.Z.Y contributed to the funding acquisition and supervised the entire project.

Conflict of interest statement: The authors declare no conflicts of interest.

References

1.   Cornell SE. Atmospheric nitrogen deposition: revisiting the question of the importance of the organic component. *Environ Pollut*. 2011; **159**(10): 2214-2222. doi: 10.1016/j.envpol.2010.11.014

2.   Jickells T, Baker AR, Cape JN *et al.* The cycling of organic nitrogen through the atmosphere. *Philos T R Soc B*. 2013; **368**(1621). doi: 10.1098/rstb.2013.0115

3.   van Breemen N. Nitrogen cycle - natural organic tendency. *Nature*. 2002; **415**(6870): 381-382. doi: 10.1038/415381a

4.   Hutchins DA, Capone DC. The marine nitrogen cycle: new developments and global change. *Nat Rev Microbiol*. 2022: 401–414. doi: 10.1038/s41579-022-00687-z

5.   Voss M, Hietanen S. The depths of nitrogen cycling. *Nature*. 2013; **493**(7434): 616-618. doi: 10.1038/493616a

6.   Zhu Q, Zhuang Q. Modeling the effects of organic nitrogen uptake by plants on the carbon cycling of boreal forest and tundra ecosystems. *Biogeosciences*. 2013; **10**(12): 7943-7955. doi: 10.5194/bg-10-7943-2013

7.   Simkin SM, Allen EB, Bowman WD *et al.* Conditional vulnerability of plant diversity to atmospheric nitrogen deposition across the United States. *PNAS*. 2016; **113**(15): 4086-4091. doi: 10.1073/pnas.1515241113

8.   Zhang Y, Forrister H, Liu J *et al.* Top-of-atmosphere radiative forcing affected by brown carbon in the upper troposphere. *Nat Geosci*. 2017; **10**(7): 486-489. doi: 10.1038/ngeo2960

9.   Duce RA, LaRoche J, Altieri K *et al.* Impacts of atmospheric anthropogenic nitrogen on the open ocean. *Science*. 2008; **320**(5878): 893-897. doi: 10.1126/science.1150369

10.   Kanakidou M, Duce RA, Prospero JM *et al.* Atmospheric fluxes of organic N and P to the global ocean. *Global Biogeochem Cy*. 2012; **26**: 1-12. doi: 10.1029/2011gb004277

11.   Kanakidou M, Myriokefalitakis S, Daskalakis N *et al.* Past, present, and future atmospheric nitrogen deposition. *J Atmos Sci*. 2016; **73**(5): 2039-2047. doi: 10.1175/jas-d-15-0278.1

12.   Cape J, Cornell S, Jickells T *et al.* Organic nitrogen in the atmosphere—Where does it come from? A review of sources and methods. *Atmos Res*. 2011; **102**(1-2): 30-48. doi: 10.1016/j.atmosres.2011.07.009

13.   Seitzinger SP, Sanders RW, Styles R. Bioavailability of DON from natural and anthropogenic sources to estuarine plankton. *Limnol Oceanogr*. 2002; **47**(2): 353-366. doi: 10.4319/lo.2002.47.2.0353

14.   Petrone KC, Richards JS, Grierson PF. Bioavailability and composition of dissolved organic carbon and nitrogen in a near coastal catchment of south-western Australia. *Biogeochemistry*. 2009; **92**(1-2): 27-40. doi: 10.1007/s10533-008-9238-z

15.   Xiu B, Liang S-k, He X-l *et al.* Bioavailability of dissolved organic nitrogen and its uptake by Ulva prolifera: implications in the outbreak of a green bloom off the coast of Qingdao, China. *Mar Pollut Bull*. 2019; **140**: 563-572. doi: 10.1016/j.marpolbul.2019.01.057

16.   Li M, Li KQ, Chen K *et al.* Size-based bioavailability of land-based DON and its impact on eutrophication of Jiaozhou bay. *Mar Pollut Bull*. 2020; **152**. doi: 10.1016/j.marpolbul.2020.110898

17.   Zhai TE, Zhang JT, Huo SL *et al.* Algal activity of dissolved organic nitrogen (DON) in the sediments of Lake Taihu, Eastern China. *Environ Earth Sci*. 2016; **75**(24). doi: 10.1007/s12665-016-6286-x

18.   Laskin A, Lin P, Laskin J *et al.* Molecular Characterization of Atmospheric Brown Carbon. *Multiphase Environmental Chemistry in the Atmosphere*. 2018; **1299**: 261-274. doi: 10.1021/bk-2018-1299.ch013

19.   Laskin A, Laskin J, Nizkorodov SA. Chemistry of Atmospheric Brown Carbon. *Chem Rev*. 2015; **115**(10): 4335-4382. doi: 10.1021/cr5006167

20.   Li J, Carlson BE, Yung YL *et al.* Scattering and absorbing aerosols in the climate system. *Nat Rev Earth Env*. 2022; **3**(6): 363-379. doi: 10.1038/s43017-022-00296-7

21.   Cheng Y, Li S-M, Leithead A. Chemical characteristics and origins of nitrogen-containing organic compounds in $PM_{2.5}$ aerosols in the Lower Fraser Valley. *Environ Sci Technol*. 2006; **40**(19): 5846-5852. doi: 10.1021/es0603857

22.   Mace KA, Artaxo P, Duce RA. Water-soluble organic nitrogen in Amazon Basin aerosols during the dry (biomass burning) and wet seasons. *J Geophys Res-Atmos*. 2003; **108**(D16). doi: 10.1029/2003jd003557

23.   Miyazaki Y, Kawamura K, Sawano M. Size distributions of organic nitrogen and carbon in remote marine aerosols: Evidence of marine biological origin based on their isotopic ratios. *Geophys Res Lett*. 2010; **37**. doi: 10.1029/2010gl042483

24.   Wang GH, Zhou BH, Cheng CL *et al.* Impact of Gobi desert dust on aerosol chemistry of Xi'an, inland China during spring 2009: differences in composition and size distribution between the urban ground surface and the mountain atmosphere. *Atmos Chem Phys*. 2013; **13**(2): 819-835. doi: 10.5194/acp-13-819-2013

25.   Perring AE, Pusede SE, Cohen RC. An observational perspective on the atmospheric impacts of alkyl and multifunctional nitrates on ozone and secondary organic aerosol. *Chem Rev*. 2013; **113**(8): 5848-5870. doi: 10.1021/cr300520x

26.   Fisher JA, Jacob DJ, Travis KR *et al.* Organic nitrate chemistry and its implications for nitrogen budgets in an isoprene- and monoterpene-rich atmosphere: constraints from aircraft (SEAC^{4}RS) and ground-based (SOAS) observations in the Southeast US. *Atmos Chem Phys*. 2016; **16**(9): 5969-5991. doi: 10.5194/acp-16-5969-2016

27.   Harrison MAJ, Barra S, Borghesi D *et al.* Nitrated phenols in the atmosphere: a review. *Atmos Environ*. 2005; **39**(2): 231-248. doi: 10.1016/j.atmosenv.2004.09.044

28.   Yuan B, Liggio J, Wentzell J *et al.* Secondary formation of nitrated phenols: insights from observations during the Uintah Basin Winter Ozone Study (UBWOS) 2014. *Atmos Chem Phys*. 2016; **16**(4): 2139-2153. doi: 10.5194/acp-16-2139-2016

29.   Wang Y, Hu M, Wang Y *et al.* The formation of nitro-aromatic compounds under high NO_x and anthropogenic VOC conditions in urban Beijing, China. *Atmos Chem Phys*. 2019; **19**(11): 7649-7665. doi: 10.5194/acp-19-7649-2019

30.   Noziere B, Dziedzic P, Cordova A. Products and kinetics of the liquid-phase reaction of glyoxal catalyzed by ammonium ions (NH_4^+). *J Phys Chem A*. 2009; **113**(1): 231-237. doi: 10.1021/jp8078293

31.   Yu G, Bayer AR, Galloway MM *et al.* Glyoxal in aqueous ammonium sulfate solutions: products, kinetics and hydration effects. *Environ Sci Technol*. 2011; **45**(15): 6336-6342. doi: 10.1021/es200989n

32.   Kua J, Krizner HE, De Haan DO. Thermodynamics and kinetics of imidazole formation from glyoxal, methylamine, and formaldehyde: A computational study. *J Phys Chem A*. 2011; **115**(9): 1667-1675. doi: 10.1021/jp111527x

33.   Sedehi N, Takano H, Blasic VA *et al.* Temperature- and pH-dependent aqueous-phase kinetics of the reactions of glyoxal and methylglyoxal with atmospheric amines and ammonium sulfate. *Atmos Environ*. 2013; **77**: 656-663. doi: 10.1016/j.atmosenv.2013.05.070

34.   Galloway MM, Powelson MH, Sedehi N *et al.* Secondary organic aerosol formation during evaporation of droplets containing atmospheric aldehydes, amines, and ammonium sulfate. *Environ Sci Technol*. 2014; **48**(24): 14417-14425. doi: 10.1021/es5044479

35.   Ito A, Lin GX, Penner JE. Reconciling modeled and observed atmospheric deposition of soluble organic nitrogen at coastal locations. *Global Biogeochem Cy*. 2014; **28**(6): 617-630. doi: 10.1002/2013gb004721

36. Ito A, Lin GX, Penner JE. Global modeling study of soluble organic nitrogen from open biomass burning. *Atmos Environ*. 2015; **121**: 103-112. doi: 10.1016/j.atmosenv.2015.01.031

37. Bey I, Jacob DJ, Yantosca RM *et al.* Global modeling of tropospheric chemistry with assimilated meteorology: model description and evaluation. *J Geophys Res-Atmos*. 2001; **106**(D19): 23073-23095. doi: 10.1029/2001jd000807

38. Singh GK, Rajeev P, Paul D *et al.* Chemical characterization and stable nitrogen isotope composition of nitrogenous component of ambient aerosols from Kanpur in the Indo-Gangetic Plains. *Sci Total Environ*. 2021; **763**. doi: 10.1016/j.scitotenv.2020.143032

39. Liu Q, Liu Y, Zhao Q *et al.* Increases in the formation of water soluble organic nitrogen during Asian dust storm episodes. *Atmos Res*. 2021; **253**. doi: 10.1016/j.atmosres.2021.105486

40. Fu T-M, Jacob DJ, Wittrock F *et al.* Global budgets of atmospheric glyoxal and methylglyoxal, and implications for formation of secondary organic aerosols. *J Geophys Res-Atmos*. 2008; **113**(D15). doi: 10.1029/2007jd009505

41. Myriokefalitakis S, Vrekoussis M, Tsigaridis K *et al.* The influence of natural and anthropogenic secondary sources on the glyoxal global distribution. *Atmos Chem Phys*. 2008; **8**(16): 4965-4981. doi: 10.5194/acp-8-4965-2008

42. Yu K, Zhu Q, Du K *et al.* Characterization of nighttime formation of particulate organic nitrates based on high-resolution aerosol mass spectrometry in an urban atmosphere in China. *Atmos Chem Phys*. 2019; **19**(7): 5235-5249. doi: 10.5194/acp-19-5235-2019

43. Huang W, Yang Y, Wang Y *et al.* Exploring the inorganic and organic nitrate aerosol formation regimes at a suburban site on the North China Plain. *Sci Total Environ*. 2021; **768**. doi: 10.1016/j.scitotenv.2020.144538

44. Lin CS, Huang RJ, Duan J *et al.* Primary and Secondary Organic Nitrate in Northwest China: A Case Study. *Environ Sci Tech Let*. 2021; **8**(11): 947-953. doi: 10.1021/acs.estlett.1c00692

45. Xu L, Suresh S, Guo H *et al.* Aerosol characterization over the southeastern United States using high-resolution aerosol mass spectrometry: spatial and seasonal variation of aerosol composition and sources with a focus on organic nitrates. *Atmos Chem Phys*. 2015; **15**(13): 7307-7336. doi: 10.5194/acp-15-7307-2015

46. Rollins AW, Browne EC, Min KE *et al.* Evidence for NOx Control over Nighttime SOA Formation. *Science*. 2012; **337**(6099): 1210-1212. doi: 10.1126/science.1221520

47. Kiendler-Scharr A, Mensah AA, Friese E *et al.* Ubiquity of organic nitrates from nighttime chemistry in the European submicron aerosol. *Geophys Res Lett*. 2016; **43**(14): 7735-7744. doi: 10.1002/2016gl069239

48. Day DA, Campuzano-Jost P, Nault BA *et al.* A systematic re-evaluation of methods for quantification of bulk particle-phase organic nitrates using real-time aerosol mass spectrometry. *Atmos Meas Tech*. 2022; **15**(2): 459-483. doi: 10.5194/amt-15-459-2022

49. Ng NL, Brown SS, Archibald AT *et al.* Nitrate radicals and biogenic volatile organic compounds: oxidation, mechanisms, and organic aerosol. *Atmos Chem Phys*. 2017; **17**(3): 2103-2162. doi: 10.5194/acp-17-2103-2017

50. Ayres BR, Allen HM, Draper DC *et al.* Organic nitrate aerosol formation via NO3 + biogenic volatile organic compounds in the southeastern United States. *Atmos Chem Phys*. 2015; **15**(23): 13377-13392. doi: 10.5194/acp-15-13377-2015

51. Fry JL, Draper DC, Barsanti KC *et al.* Secondary Organic Aerosol Formation and Organic Nitrate Yield from NO3 Oxidation of Biogenic Hydrocarbons. *Environ Sci Technol*. 2014; **48**(20): 11944-11953. doi: 10.1021/es502204x

52. Boyd CM, Sanchez J, Xu L *et al.* Secondary organic aerosol formation from the beta-pinene+NO3 system: effect of humidity and peroxy radical fate. *Atmos Chem Phys*. 2015; **15**(13): 7497-7522. doi: 10.5194/acp-15-7497-2015

53.   Darer AI, Cole-Filipiak NC, O'Connor AE *et al.* Formation and Stability of Atmospherically Relevant Isoprene-Derived Organosulfates and Organonitrates. *Environ Sci Technol.* 2011; **45**(5): 1895-1902. doi: 10.1021/es103797z

54.   Wang Y, Piletic IR, Takeuchi M *et al.* Synthesis and Hydrolysis of Atmospherically Relevant Monoterpene-Derived Organic Nitrates. *Environ Sci Technol.* 2021; **55**(21): 14595-14606. doi: 10.1021/acs.est.1c05310

55.   Takeuchi M, Ng NL. Chemical composition and hydrolysis of organic nitrate aerosol formed from hydroxyl and nitrate radical oxidation of alpha-pinene and beta-pinene. *Atmos Chem Phys.* 2019; **19**(19): 12749-12766. doi: 10.5194/acp-19-12749-2019

56.   Wang Y, Takeuchi M, Wang S *et al.* Photolysis of Gas-Phase Atmospherically Relevant Monoterpene- Derived Organic Nitrates. *J Phys Chem A.* 2023; **127**(4): 987-999. doi: 10.1021/acs.jpca.2c04307

57.   Muller JF, Peeters J, Stavrakou T. Fast photolysis of carbonyl nitrates from isoprene. *Atmos Chem Phys.* 2014; **14**(5): 2497-2508. doi: 10.5194/acp-14-2497-2014

58.   Yu X, Pan Y, Song W *et al.* Wet and dry nitrogen depositions in the Pearl River Delta, South China: observations at three typical sites with an emphasis on water-soluble organic nitrogen. *J Geophys Res-Atmos.* 2020; **125**(3). doi: 10.1029/2019jd030983

59.   Nakamura T, Narita Y, Kanazawa K *et al.* Organic nitrogen of atmospheric aerosols in the coastal area of Seto Inland Sea. *Aerosol Air Qual Res.* 2020; **20**(5): 1016-1025. doi: 10.4209/aaqr.2019.12.0658

60.   Browne EC, Perring AE, Wooldridge PJ *et al.* Global and regional effects of the photochemistry of CH3O2NO2: evidence from ARCTAS. *Atmos Chem Phys.* 2011; **11**(9): 4209-4219. doi: 10.5194/acp-11-4209-2011

61.   Fischer EV, Jacob DJ, Yantosca RM *et al.* Atmospheric peroxyacetyl nitrate (PAN): a global budget and source attribution. *Atmos Chem Phys.* 2014; **14**(5): 2679-2698. doi: 10.5194/acp-14-2679-2014

62.   Du E, Terrer C, Pellegrini AFA *et al.* Global patterns of terrestrial nitrogen and phosphorus limitation. *Nat Geosci.* 2020; **13**(3): 221. doi: 10.1038/s41561-019-0530-4

63.   Bronk DA, See JH, Bradley P *et al.* DON as a source of bioavailable nitrogen for phytoplankton. *Biogeosciences.* 2007; **4**(3): 283-296. doi: 10.5194/bg-4-283-2007

64.   Bauters M, Drake TW, Verbeeck H *et al.* High fire-derived nitrogen deposition on central African forests. *PNAS.* 2018; **115**(3): 549-554. doi: 10.1073/pnas.1714597115

65.   Aranguren-Gassis M, Kremer CT, Klausmeier CA *et al.* Nitrogen limitation inhibits marine diatom adaptation to high temperatures. *Ecol Lett.* 2019; **22**(11): 1860-1869. doi: 10.1111/ele.13378

66.   Ardyna M, Arrigo KR. Phytoplankton dynamics in a changing Arctic Ocean. *Nat Clim Change.* 2020; **10**(10): 892-903. doi: 10.1038/s41558-020-0905-y

67.   Lewis KM, van Dijken GL, Arrigo KR. Changes in phytoplankton concentration now drive increased Arctic Ocean primary production. *Science.* 2020; **369**(6500): 198. doi: 10.1126/science.aay8380

68.   Tang W, Llort J, Weis J *et al.* Widespread phytoplankton blooms triggered by 2019-2020 Australian wildfires. *Nature.* 2021; **597**(7876): 370-375. doi: 10.1038/s41586-021-03805-8

69.   Zheng B, Ciais P, Chevallier F *et al.* Increasing forest fire emissions despite the decline in global burned area. *Sci Adv.* 2021; **7**(39). doi: 10.1126/sciadv.abh2646

70.   Li Y, Schichtel BA, Walker JT *et al.* Increasing importance of deposition of reduced nitrogen in the United States. *PNAS.* 2016; **113**(21): 5874-5879. doi: 10.1073/pnas.1525736113

71.   Li G, Cheng L, Zhu J *et al.* Increasing ocean stratification over the past half-century. *Nat Clim Change.* 2020; **10**(12): 1116-1123. doi: 10.1038/s41558-020-00918-2
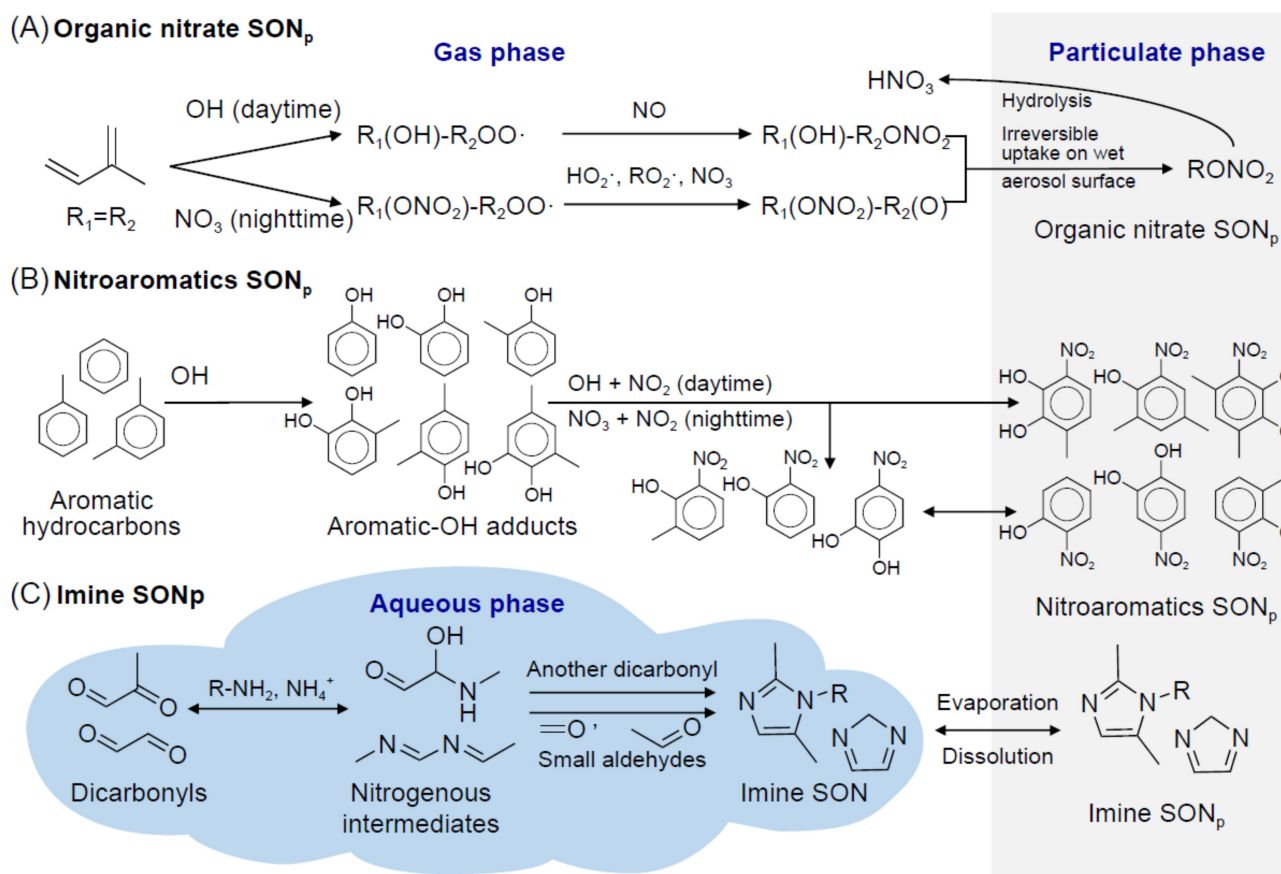
Fig. 1. Schematic diagram of the three particulate secondary ON (SON$_p$) formation pathways included in this study. (A) SON$_p$ as part of organic nitrates (RONO$_2$) produced by the oxidation of volatile organic compounds by OH or NO$_3$ radicals in the presence of NO$_x$, (B) SON$_p$ as part of nitroaromatics (NACs) produced by the oxidation of aromatic compounds by OH and NO$_3$ radicals in the presence of NO$_x$, and (C) SON$_p$ as part of imine-like compounds produced by the aqueous reactions of dicarbonyls with ammonium or amines. One-way arrows indicate irreversible reactions from precursors to products; double arrows indicate reversible reactions.
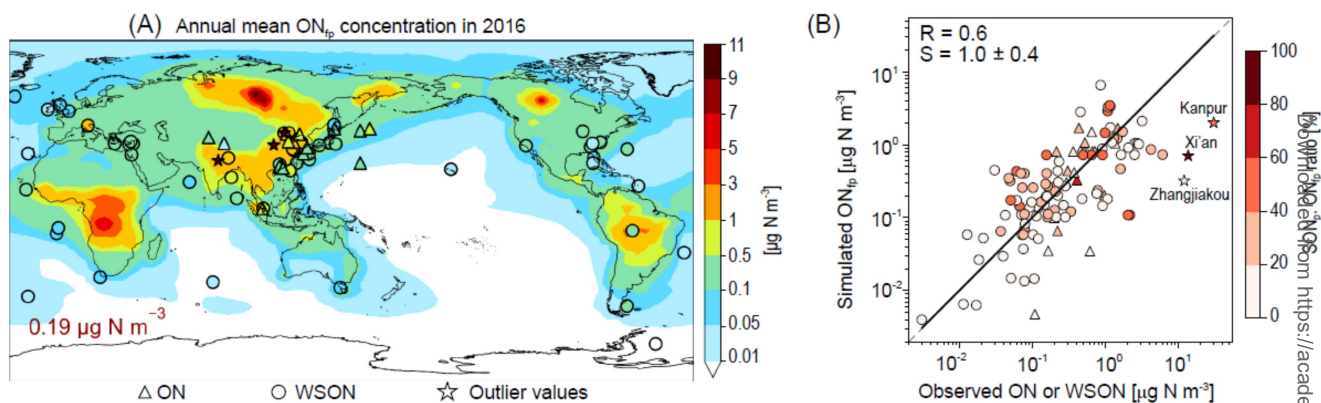
Fig. 2. Observed and simulated global annual mean surface ON$_{fp}$ concentrations. Observations shown as symbols; triangles: ON measurements; circles: water-soluble ON (WSON) measurements; stars: outliers affected by strong local, intermittent sources. (**A**) Observed (symbols) and simulated (filled contours) annual mean surface ON$_{fp}$ concentrations. The simulated global annual mean surface ON$_{fp}$ concentration is shown inset. (**B**) Scatterplot of simulated versus observed annual mean surface ON$_{fp}$ concentrations, color-coded by the SON$_p$:ON$_{fp}$ ratios. Black line indicates the reduced major axis regression line, excluding the three outliers. Grey dashed line indicates the 1:1 line. The slope (S) and correlation coefficient (R) are shown inset.
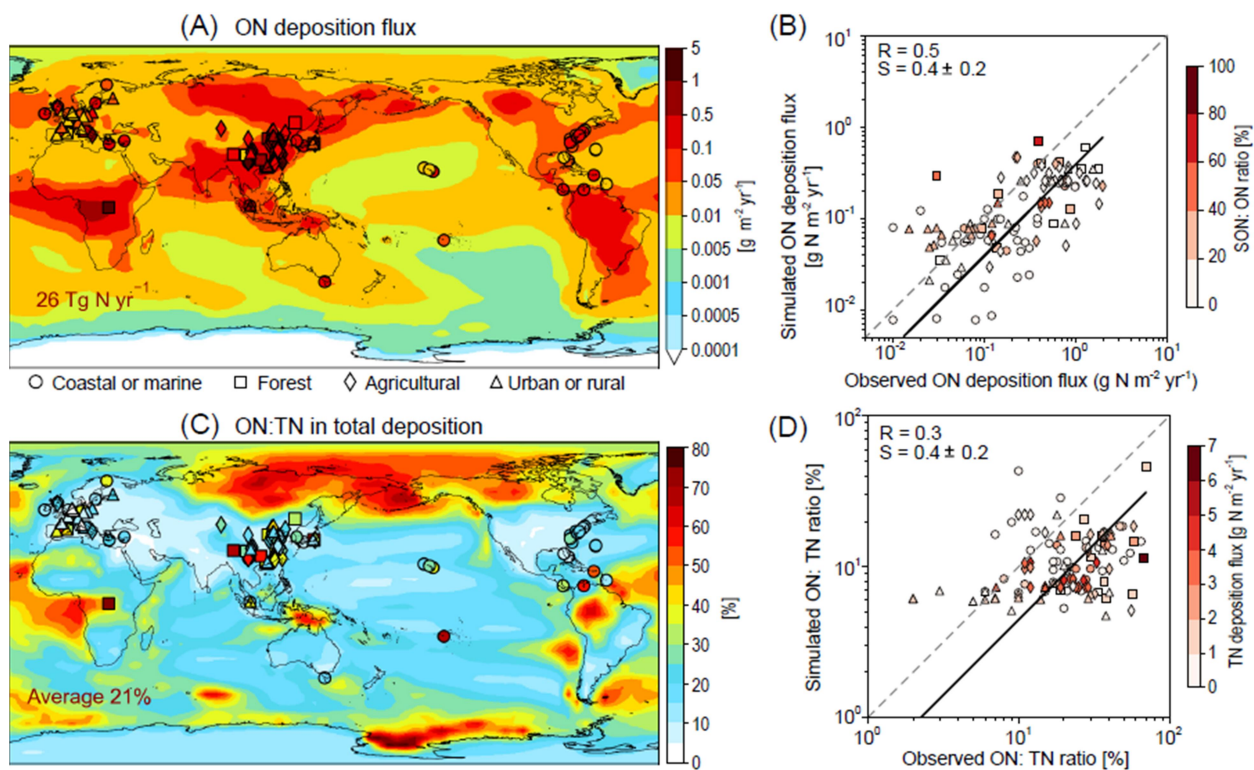
Fig. 3. Observed and simulated atmospheric ON deposition fluxes and the ON:TN ratios in atmospheric deposition fluxes. (A) Observed (symbols) and simulated (filled contours) ON deposition fluxes; (B) Scatterplot of (A); (C) Observed and simulated ON:TN ratios in atmospheric deposition fluxes. (D) Scatterplot of (C). The black lines indicate the reduced major axis regression lines; the grey dashed lines show the 1:1 lines. The symbol colors in (B) indicate the simulated SON mass fraction in the total ON deposition flux at each site. The symbol colors in (D) indicate the simulated TN deposition fluxes.
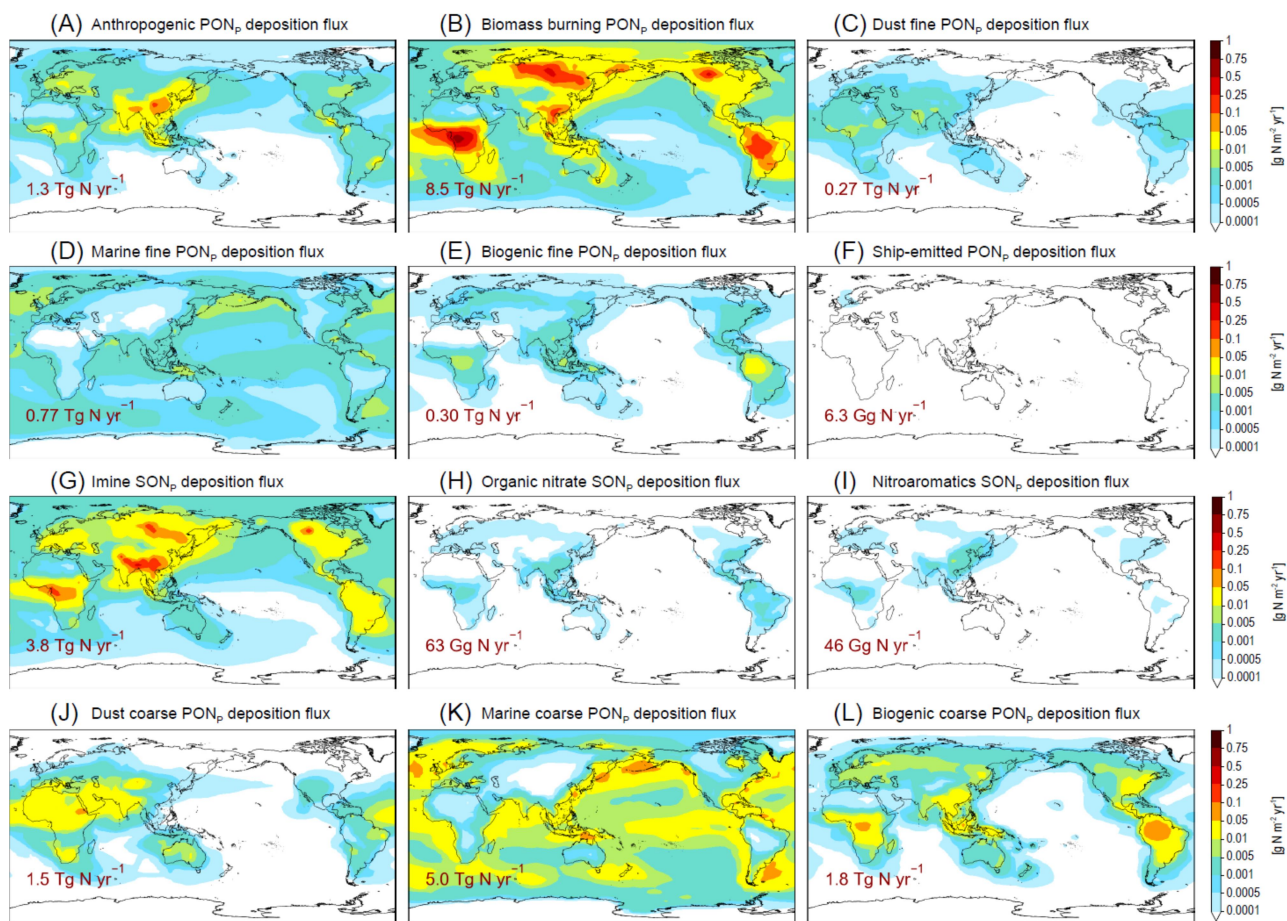
Fig. 4. Simulated annual mean atmospheric deposition fluxes of ON$_p$ from different sources. (**A**) anthropogenic PON$_p$; (**B**) biomass burning PON$_p$; (**C**) fine dust PON$_p$; (**D**) fine marine PON$_p$; (**E**) fine biogenic PON$_p$; (**F**) ship-emitted PON$_p$; (**G**) imine SON$_p$; (**H**) organic nitrate SON$_p$; (**I**) nitroaromatic SON$_p$; (**J**) coarse dust PON$_p$; (**K**) coarse marine PON$_p$; (**L**) coarse biogenic PON$_p$.
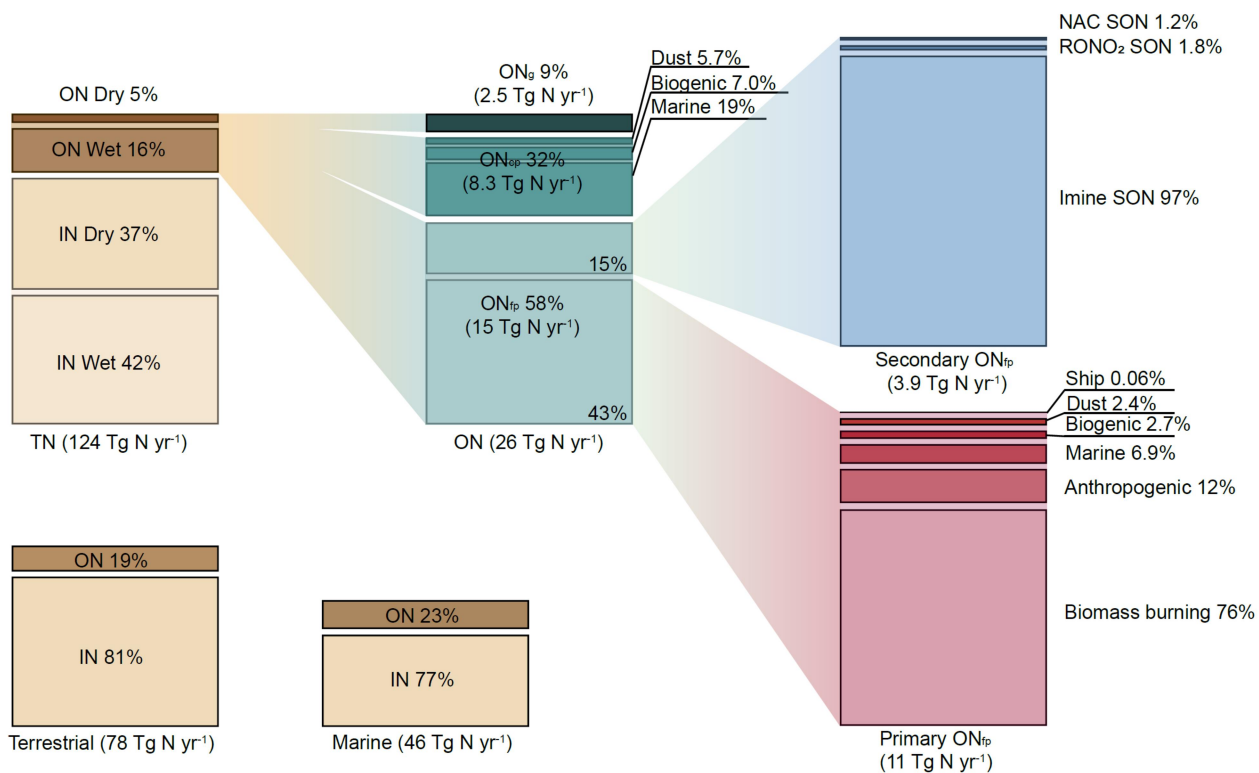
Fig. 5. The global atmospheric TN deposition flux and the contributions of different N components as simulated by this study.
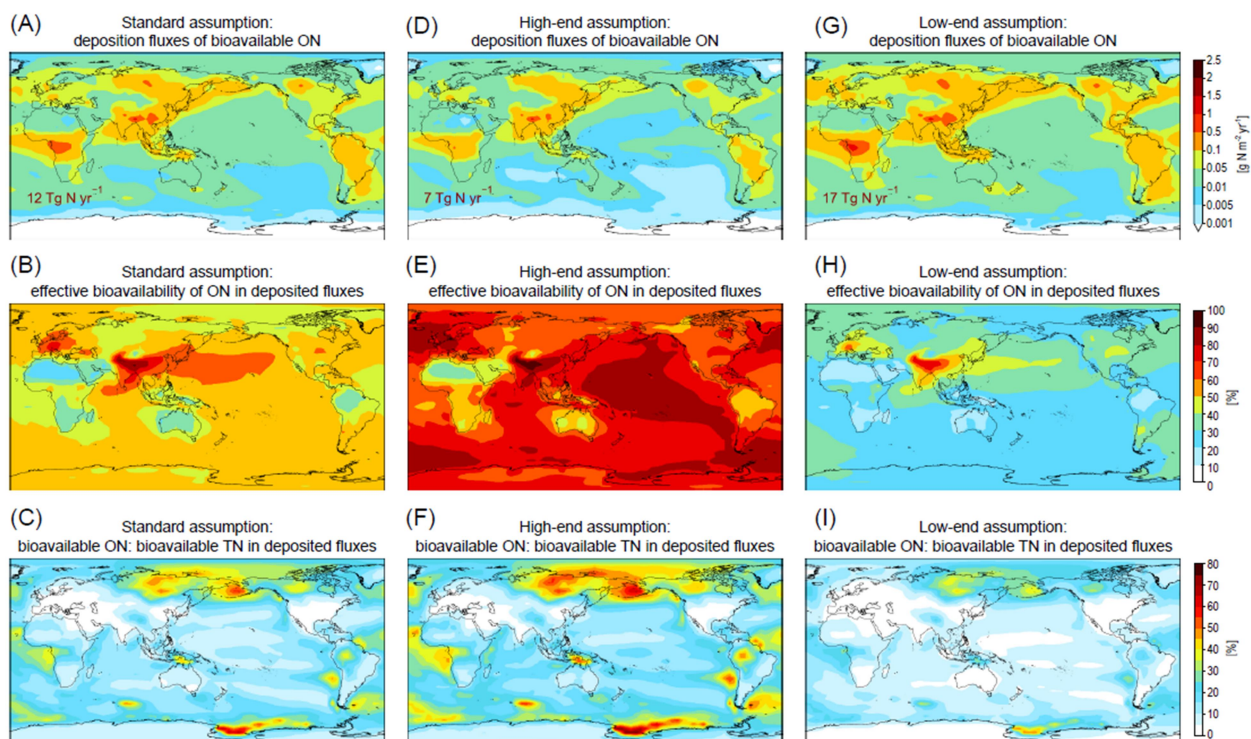
Fig. 6. Spatial distribution of bioavailable ON deposition fluxes from the atmosphere. **(A, D, G)** simulated atmospheric deposition fluxes of bioavailable ON; **(B, E, H)** the effective bioavailability of ON in the deposited fluxes; **(C, F, I)** the ratios of bioavailable ON versus bioavailable TN in the deposition fluxes. The left column shows the results from our standard assumption on ON bioavailability. The middle and right columns show the results assuming high-end and low-end values of ON bioavailability, respectively (Supplementary Materials: Text S3). The global atmospheric bioavailable ON deposition fluxes are shown inset.

Table 1. Global budget of atmospheric ON and the ON:TN ratios in atmospheric deposition as simulated by the GEOS-Chem model.

Source types	Atmospheric burden [Tg N]	Emission [Tg N yr^{-1}]	Net chemical production[a] [Tg N yr^{-1}]	Dry deposition[b] [Tg N yr^{-1}]	Wet deposition[b] [Tg N yr^{-1}]	Total deposition[b] [Tg N yr^{-1}]	Total deposition to the ocean[b] [Tg N yr^{-1}]
Total ON (ON$_p$ + ON$_g$)	1.3	20	5.8	6.0 (5.0)	20 (17)	26 (22)	11 (8.0)
Particulate ON (ON$_p$)	0.31	19	3.9	4.0 (3.0)	19 (17)	23 (20)	10 (7.5)
Fine mode (ON$_{fp}$)							
Anthropogenic emissions	0.021	1.3	-	0.29 (0.23)	1.0 (1.0)	1.3 (1.2)	0.51 (0.47)
Biomass burning emissions	0.16	8.5	-	1.7 (1.4)	6.7 (6.5)	8.5 (7.9)	2.4 (2.3)
Dust emissions	0.0079	0.27	-	0.059 (0.042)	0.21 (0.20)	0.27 (0.24)	0.11 (0.10)
Primary biological particle emissions	0.0070	0.30	-	0.053 (0.053)	0.25 (0.25)	0.30 (0.30)	0.074 (0.074)
Ship emissions	0.000062	0.0063	-	0.0016 (0.0012)	0.0047 (0.0043)	0.0063 (0.0055)	0.0049 (0.0049)
Marine emissions	0.0032	0.77	-	0.22 (0.12)	0.55 (0.45)	0.77 (0.57)	0.65 (0.46)
Organic nitrate SON$_p$	0.00080	-	0.069	0.028 (0.028)	0.040 (0.040)	0.068 (0.068)	0.016 (0.016)
NAC SON$_p$	0.00082	-	0.046	0.011 (0.011)	0.035 (0.035)	0.046 (0.046)	0.015 (0.015)
Imine SON$_p$	0.065	-	3.8	0.56 (0.56)	3.2 (3.2)	3.8 (3.8)	0.98 (0.98)
Coarse mode (ON$_{cp}$)							
Dust emissions	0.023	1.5	-	0.22 (0.14)	1.3 (1.0)	1.5 (1.1)	0.44 (0.40)
Primary biological particle emissions	0.0056	1.8	-	0.13 (0.13)	1.7 (1.7)	1.8 (1.8)	0.33 (0.33)
Marine emissions	0.014	5.0	-	0.63 (0.31)	4.4 (2.3)	5.0 (2.6)	4.6 (2.4)
Gaseous ON (ON$_g$)	1.0	0.75	1.7	2.0 (2.0)	0.45 (0.41)	2.5 (2.5)	0.49 (0.49)
ON:TN in deposited fluxes	-	-	-	11% (10%)	28% (25%)	21% (18%)	23% (18%)

[a] Net chemical production indicates the net effect of chemical production and loss process.

[b] Soluble ON fluxes shown in parentheses.